
CAFA: Class-Aware Feature Alignment for Test-Time Adaptation

Sanghun Jung¹ Jungsoo Lee^{1,2} Nanhee Kim³ Jaegul Choo¹

¹KAIST AI, ²Kakao Enterprise, ³Enssel Inc., South Korea

¹{shjung13, bebeto, jchoo}@kaist.ac.kr,

²bebeto.lee@kakaenterprise.com, ³nhkim@enssel.com

Abstract

Despite recent advancements in deep learning, deep networks still suffer from performance degradation when they face new and different data from their training distributions. Addressing such a problem, test-time adaptation (TTA) aims to adapt a model to unlabeled test data on test time while making predictions simultaneously. TTA applies to pretrained networks without modifying their training procedures, which enables to utilize the already well-formed source distribution for adaptation. One possible approach is to align the representation space of test samples to the source distribution (*i.e.*, feature alignment). However, performing feature alignments in TTA is especially challenging in that the access to labeled source data is restricted during adaptation. That is, a model does not have a chance to learn test data in a class-discriminative manner, which was feasible in other adaptation tasks (*e.g.*, unsupervised domain adaptation) via supervised loss on the source data. Based on such an observation, this paper proposes *a simple yet effective* feature alignment loss, termed as Class-Aware Feature Alignment (CAFA), which 1) encourages a model to learn target representations in a class-discriminative manner and 2) effectively mitigates the distribution shifts in test time, simultaneously. Our method does not require any hyper-parameters or additional losses, which are required in the previous approaches. We conduct extensive experiments and show our proposed method consistently outperforms existing baselines.

1 Introduction

Recent advancements [1, 2, 3, 4] in machine learning have demonstrated their effectiveness in solving diverse problems, achieving remarkable performance enhancements on benchmarking datasets. However, they suffer from significant performance degradation when they face test data with different conditions from their training data (*i.e.*, source data), such as corruptions [5], light changes [6], or adverse weather [7, 8]. Such sensitivity to distribution shifts [9] hampers deep networks from performing well in the practical scenarios since test samples may include such distribution shifts [10]. Thus, adapting deep models to the test samples is crucial, especially when there exist distribution shifts.

To alleviate such problems, various adaptation methods have been proposed [11, 12, 13, 14, 15, 16, 17, 18]. However, most of them require either access to the source data during adaptation or modification of the training procedure, which limits their applicability (*e.g.*, data privacy issues limit the use of source data). Addressing such concerns, we pursue to design an adaptation method that 1) is applicable to existing deep networks without modification and 2) does not require access to the source data during adaptation. In order to satisfy such conditions, previous studies perform adaptation on test time while making predictions simultaneously, which is referred to as *test-time adaptation* (TTA).

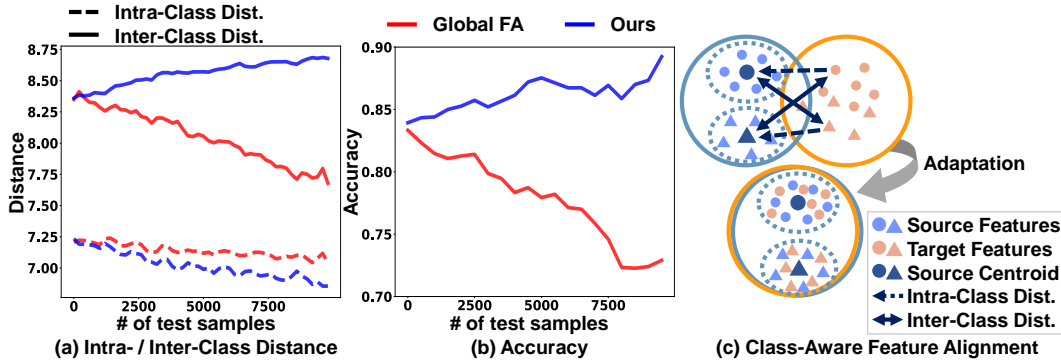


Figure 1: A motivating example of our paper. (a) shows the change of the intra-class distance (dotted lines) and the inter-class distance (solid lines) of ours (blue line) and global feature alignment (red line). (b) shows the accuracy changes as adaptation proceeds. (c) illustrates how our method CAFA aligns the test features to source class-conditional distributions. Plots are obtained from the Gaussian noise corruption with severity level 5 in the CIFAR10-C dataset.

One of the widely adopted approaches to address distribution shifts is aligning the source (*i.e.*, train data) and target (*i.e.*, test data) distributions [14, 15, 19, 20, 16, 21]. DANN [14] directly reduces \mathcal{H} -divergence between the source and target distributions, and CORAL [15] minimizes the difference of the second-order statistics between the source and target data. Despite their demonstrated effectiveness in other adaptation tasks, applying those alignments to TTA bears the following limitation. They generally perform alignments with supervised losses on the source data, which encourages a model to learn target distributions in a class-discriminative manner [15]. However, access to the source data is prohibited in TTA, limiting a model from learning class-discriminability.

Considering such an issue, we conduct an analysis on the effects of feature alignments in TTA by using two distances in the representation space: intra-class distance and inter-class distance. As shown in Fig. 1 (c), intra-class distance (dotted arrow) is defined as the distance between a sample and its ground-truth source class distribution, and inter-class distance (solid arrow) denotes the averaged distance between the sample and other source class distributions. Obviously, achieving low intra-class distance and high inter-class distance is crucial for improving classification accuracy [22, 23, 24, 25, 26]. We first align the target distribution to the source distribution without considering class information (Fig. 1 (a) (red lines)). We term this alignment as global feature alignment in our paper. As shown, intra-class distance is reduced, which is desirable, but it also accompanies the decrease of inter-class distance. Such effects degrade the image classification accuracy in Fig. 1 (b) (red line). This is mainly because there is no chance for a model to learn the test data in a class-discriminative manner since a supervised loss is not available both on the source and target data. To improve the class-discriminability of a model, we further consider the class information by 1) enlarging the inter-class distance and 2) reducing the intra-class distance as shown in Fig. 1 (a) (blue lines). Such an approach significantly improves the classification accuracy as adaptation proceeds, as illustrated in Fig. 1 (b) (blue line).

Motivated by such observations, we propose Class-Aware Feature Alignment (CAFA) which aligns the target features to the pre-calculated source feature distribution by considering both intra- and inter-class distances. To be more specific, we pre-calculate the statistics (*i.e.*, mean and covariance) of the source distribution to estimate class-conditional Gaussian distributions from source samples using a pretrained network. In test-time adaptation, we utilize the Mahalanobis distance to 1) align each sample to its predicted class-conditional Gaussian distribution (*i.e.*, reduce intra-class distance) and 2) enforce samples to be distinct from other class-conditional Gaussian distributions (*i.e.*, increase inter-class distance).

The main contributions of our work are as follows:

- We propose a novel Class-Aware Feature Alignment (CAFA) that effectively mitigates the distribution shifts and encourages a model to learn discriminative target representations simultaneously.
- Our proposed approach is simple yet effective, not requiring hyper-parameters or additional modifications of the training procedure.
- We conduct extensive experiments along with in-depth analysis and show that CAFA consistently outperforms the existing baselines models on test-time adaptation.

2 Related Work

2.1 Unsupervised Domain Adaptation

Unsupervised domain adaptation (UDA) approaches [27, 28, 11, 12, 13, 29, 30, 31] have addressed distribution shifts effectively by utilizing various strategies such as adversarial training [14, 16, 21, 32, 32, 33] or minimizing the discrepancy [34, 35, 36]. However, they still assume the source data is available during adaptation, which is recently addressed by source-free UDA approaches [37, 38, 17, 39, 40, 41, 42, 43, 44, 18]. SHOT [37] utilizes the information maximization [45] loss for adaptation, and G-SFDA [46] performs local structure clustering along with domain-specific attention. While the previous source-free UDA approaches have demonstrated their effectiveness, they necessitate altering the training procedure. On the other hand, our proposed method CAFA neither requires access to the source data during adaptation nor modifies the training procedure, making our method widely applicable.

2.2 Test-time Adaptation

Unlike UDA methods that adapt to target distribution during the training phase, approaches adapting to target distributions at the test time have been proposed [47, 48, 49, 50, 51, 52, 53, 54]. Without accessing to the source data, test-time training methods [53, 54] train a model with self-supervised tasks (*e.g.*, predicting the rotation degree) and utilize them as proxy losses for adaptation. However, as also pointed out in Wang *et al.* [47], there is no guarantee that optimizing proxy losses helps in terms of the main task since they are not directly related to classifying images into different classes. Furthermore, they iterate several epochs over test samples and predict all the test data after the iteration is done. Addressing those concerns, test-time adaptation methods [47, 48, 49, 50, 51] have been proposed. They adapt a model to test data while making predictions simultaneously. These approaches do not require the modification of the training procedure. Due to such an adaptation setting, those algorithms are applicable to a given pretrained deep learning network. Recent seminal work in TTA, TENT [47], proposed to update the parameters in batch normalization [55] layers and statistics while minimizing the entropy loss. Our method CAFA follows the setting of test-time adaptation.

2.3 Feature Alignments

Feature alignment is widely adopted in UDA studies to mitigate distribution shifts [20, 16, 19, 21]. However, most of them do not consider categorical information, but rather match the source and target distributions globally. This may harm the class-discriminability since it does not guarantee the class-to-class matching between two distributions [23]. Pointing out such an issue, several approaches [23, 24, 56, 57, 25, 58, 59] proposed to align the distributions in a class-discriminative manner. This point of view also holds in the case of test-time adaptation, and we design a simple loss that effectively mitigates the distribution gap while improving class-discriminability, simultaneously.

3 Preliminary

Assume that we have a model $f_s(x) = h_s \circ g_s(x)$ pretrained with a supervised loss $\mathcal{L}(x_s, y_s)$ on source data. Here $g_s : \mathcal{X}_s \rightarrow \mathbb{R}^d$ denotes the pretrained feature extractor, and $h_s : \mathbb{R}^d \rightarrow \mathbb{R}^C$ indicates the pretrained classifier, where d is the dimension of extracted features, and C is the number of classes. Then, we aim to adapt the pretrained model $f_s(\cdot)$ to target data (x_t, y_t) while correctly classifying them during test time.

Mahalanobis distance In this work, we adopt the Mahalanobis distance to align the source and target distributions. Mahalanobis distance measures the distance between a distribution and a sample. With an input image x , feature extractor $g(\cdot)$, and Gaussian distribution $\mathcal{N}(\mu, \Sigma)$, Mahalanobis distance is defined as

$$D(x; \mu, \Sigma) = (g(x) - \mu)^\top \Sigma^{-1} (g(x) - \mu). \quad (1)$$

Intra-/inter-class distance For an in-depth analysis, we measure the intra- and inter-class distances between the class-conditional source distributions and target samples. To be more specific, we define class-conditional Gaussian distributions as $P(g_s(x)|y=c) = \mathcal{N}(g_s(x)|\mu_c, \Sigma_c)$, where μ_c, Σ_c are the mean and covariance of multivariate Gaussian distribution of class $c \in \{1, \dots, C\}$. Then, with a target image x_t , the intra-class distance is defined as

$$D_{\text{intra}}(x_t, y_t) = D(x_t; \mu_{y_t}, \Sigma_{y_t}), \quad (2)$$

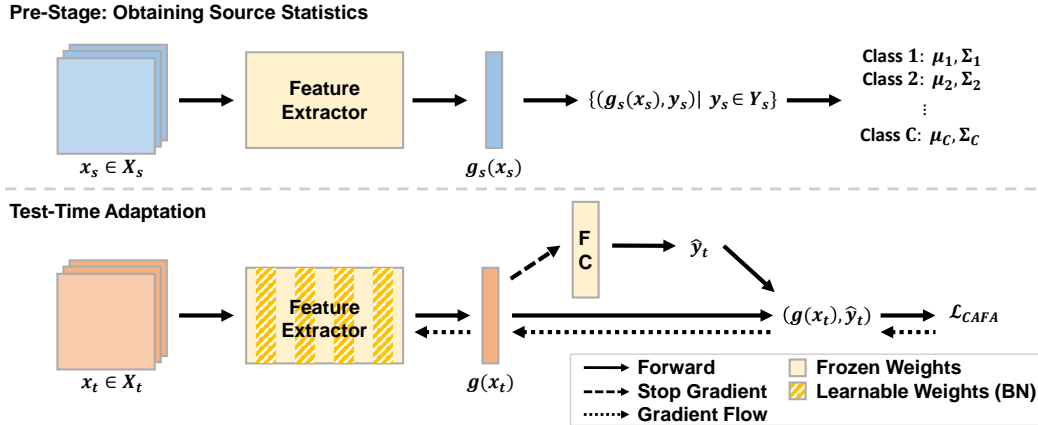


Figure 2: Overview of our method. (Pre-stage) Ours first pre-calculates the source class-conditional Gaussian distributions using a pre-trained feature extractor. (Test-time adaptation) During test-time adaptation, ours adapts a model by optimizing Class-Aware Feature Alignment (CAFA) loss while making predictions simultaneously.

where y_t indicates the corresponding ground-truth label of the target image. In the same manner, the inter-class distance is defined as

$$D_{\text{inter}}(x_t, y_t) = \frac{1}{C-1} \sum_{c=1}^C \mathbb{1}(y_t \neq c) D(x_t; \mu_c, \Sigma_c) \quad (3)$$

Note that achieving low intra-class distance and high inter-class distance is important for improving the image classification accuracy.

4 CAFA: Class-Aware Feature Alignment

This section presents an in-depth analysis on feature alignments and the details of our proposed method, CAFA. As illustrated in Fig. 2, CAFA first pre-calculates the source class-conditional Gaussian distributions using a pretrained model and adapts a model to test data during the test time by aligning the test features to obtained class-conditional Gaussian distributions.

4.1 Analysis on Class Separability in Feature Alignment

We compare and analyze three different feature alignments with respect to the intra- and inter-class distances. First, we investigate the global feature alignment that reduces the gap between the source and target distributions without considering class information. With the given source Gaussian distribution $\mathcal{N}(g_s(x_s) | \mu_s, \Sigma_s)$, the global feature alignment loss \mathcal{L}_{FA} is formulated as

$$\mathcal{L}_{\text{FA}} = \|\mu_s - \mu_t\|_2^2 + \|\Sigma_s - \Sigma_t\|_F^2, \quad (4)$$

where μ_s, Σ_s denote the mean and covariance of source features without considering class information, μ_t, Σ_t indicate the mean and covariance estimated from a mini-batch of test samples, and $\|\cdot\|_2, \|\cdot\|_F$ denote Euclidean norm and Frobenius norm, respectively. As aforementioned, while the global feature alignment drastically decreases the intra-class distance, it also accompanies a significant reduction of inter-class distance which needs to be high for achieving a reasonable level of image classification accuracy (Fig. 1 (a) (red lines)). Fig. 1 (b) also verifies such a point by visualizing the degraded image classification accuracy.

To address such a problem, we take the *class* information into account when performing the feature alignment. Aligning the source and target distributions in a class-wise manner would be one straightforward approach. However, during the test phase, there exist excessively few number of samples for each class in a mini-batch to precisely estimate class-conditional distributions of test data. Thus, we align individual test samples to the source class-conditional distribution of the predicted class by using the Mahalanobis distance. Specifically, with the given source class-conditional Gaussian distributions $\mathcal{N}(\mu_c, \Sigma_c)$, the loss $\mathcal{L}_{\text{intra}}$ minimizing the intra-class distance is defined as

$$\mathcal{L}_{\text{intra}} = \frac{1}{N} \sum_{n=1}^N D_{\text{intra}}(x_{t,n}, \hat{y}_{t,n}), \quad (5)$$

where $\hat{y}_{t,n}$ indicates the predicted label of the target sample $x_{t,n}$, and N denotes the number of target samples. While utilizing $\mathcal{L}_{\text{intra}}$ effectively reduces the intra-class distance, it still decreases the inter-class distance. We further elaborate on such a point in Section 5.2.

Finally, we also consider the inter-class distance explicitly in addition to the $\mathcal{L}_{\text{intra}}$ which we further explain in Section 4.2. The change of the intra- and inter-class distances when our final loss is applied is visualized in Fig. 1 (a) (blue lines). Our final loss desirably aligns the source and target distributions by reducing the intra-class distance and enlarging the inter-class distance. As also shown in Fig. 1(b) (red line), our final loss improves the image classification accuracy and class-discriminability compared to the global feature alignment.

4.2 Class-Aware Feature Alignment

Pre-calculation of source statistics As shown in the pre-stage of Fig. 2, we calculate C class-conditional Gaussian distributions $P(g_s(x_s)|y=c) = \mathcal{N}(g_s(x_s)|\boldsymbol{\mu}_c, \boldsymbol{\Sigma}_c)$ with the pretrained feature extractor $g_s(\cdot)$ over source training samples $(x_s, y_s) \sim \mathcal{X}_s$ with the following equations:

$$\begin{aligned} \boldsymbol{\mu}_c &= \frac{1}{N_c} \sum_{n=1}^{N_c} g_s(x_{s,n}) \\ \boldsymbol{\Sigma}_c &= \frac{1}{N_c} \sum_{n=1}^{N_c} (g_s(x_{s,n}) - \boldsymbol{\mu}_c)(g_s(x_{s,n}) - \boldsymbol{\mu}_c)^\top, \end{aligned} \tag{6}$$

where N_c denotes the number of training samples of class c . In the linear discriminant analysis (LDA), it is assumed that all the class-conditional Gaussian distributions have the same covariance matrix (*i.e.*, tied covariance). However, as also pointed out in Lee *et al.* [60], deep networks are not trained to have the same covariance across the different classes. Due to this fact, we utilize class-wise covariance matrices for our experiments. Note that even with using a tied covariance, ours still outperforms the existing baselines, and we further explain it in Section 5.2.

Test-time adaptation With the obtained source class-conditional distributions $P(g_s(x_s)|y=c)$ at the pre-stage, we perform class-aware feature alignment (CAFA) during the test time. We initialize a model using the weights of pretrained networks $f_s(\cdot)$ and perform adaptation to target data considering both intra- and inter-class distances. Our final loss $\mathcal{L}_{\text{CAFA}}$ is defined as

$$\mathcal{L}_{\text{CAFA}} = \frac{1}{N} \sum_{n=1}^N \log \frac{D_{\text{intra}}(x_{t,n}, \hat{y}_{t,n})}{\sum_{c=1}^C D(x_{t,n}; \boldsymbol{\mu}_c, \boldsymbol{\Sigma}_c)}. \tag{7}$$

5 Experiments

This section first demonstrates the evaluation results on two different settings: 1) robustness to corruptions, and 2) domain adaptation on digits. Then, we present an in-depth analysis on our method by conducting ablation studies and providing visualizations of the representation space. For corruption datasets, we evaluate models on CIFAR10-C, CIFAR100-C, TinyImageNet-C, and ImageNet-C [5] datasets. Furthermore, we measure the adaptation errors on the Office-Home [61] and digit datasets (*i.e.*, training a model on SVHN [62] and validating it on MNIST [63] / MNIST-M [64] / USPS [65] datasets).

Datasets CIFAR10 [66] and CIFAR100 [66] include 50,000 training samples and 10,000 test samples with 10 and 100 classes, respectively. CIFAR10-C and CIFAR100-C [5] datasets contain 15 different corruptions, and the corruptions are applied to the test set of CIFAR10 and CIFAR100 datasets. TinyImageNet [67] is a subset of the original ImageNet [68] dataset, containing 100,000 training images and 10,000 validation images with 200 classes. ImageNet [68] contains 1.2 million training samples and 50,000 validation samples with 1,000 object categories. Analogous to CIFAR10-C / CIFAR100-C, TinyImageNet-C and ImageNet-C are composed of 15 different corruptions, where the corruptions are applied to the validation set of TinyImageNet and ImageNet, respectively. Office-Home [61] dataset consists of around 15,500 images and contains 65 categories of everyday objects with four distinct domains: Artistic images (Ar), Clip art images (Cl), Product images (Pr), and Real-world images (Re). For the digit datasets, SVHN includes color images of house numbers collected from street views with 73,257 training samples and 26,032 test samples. We use 10,000/9,001/2,007 hand-written digit test samples from MNIST / MNIST-M / USPS, respectively. All four digit datasets have ten classes, 0-9.

Baselines For a fair comparison, we consider the following baselines in our experiments:

- Source: Evaluating the pretrained network on the test data without any adaptation.
- Test-time normalization (BN) [51] updates the batch normalization statistics [55] on test data in test time.
- Pseudo label (PL) [52] utilizes the predicted label as a label for optimizing the main task loss during testing.
- Test-time entropy minimization (TENT) [47] updates batch normalization [55] layer statistics and parameters on test data by minimizing entropy.
- Source hypothesis transfer (SHOT) [37] updates feature extractor utilizing the information maximization loss [45] with the self-supervised pseudo-labeling during test time.
- Test-time feature alignment (TFA) [54] aligns the source and target distributions by matching the first- and second-order statistics of outputs from both the penultimate layer and self-supervised task branch.
- Test-time training (TTT++) [54] updates the model by jointly aligning the first- and second-order statistics between the source and target distributions and optimizing the proxy loss (*i.e.*, contrastive loss for self-supervision task) during test time.

Note that test-time normalization (BN), pseudo label (PL), test-time entropy minimization (TENT), and CAFA (ours) are test-time adaptation methods. SHOT [37], TFA, and TTT++ [54] are originally designed for source-free UDA and test-time training, respectively. They iterate multiple epochs on the entire test samples during test time.

Implementation details For all experiments, we adopt the residual networks [1] with 50 layers (ResNet-50). We train the model by following the same training protocol described in TTT++ [54] for the corruption datasets except for the ImageNet-C dataset. For experiments on ImageNet-C, we adopt the pretrained ResNet-50 networks provided by Pytorch [69]. For the digit datasets, we do not apply the joint training step with a self-supervised task. To make a fair comparison for each experiment, we use the same network and pretrained weight for all the baselines in the same experiment condition. For test-time adaptation, we only optimize the batch normalization parameters γ, β , following Wang *et al.* [47]. We set the batch size as 200 and utilize Adam [70] optimizer with the learning rate of 0.001 for adaptation except for the ImageNet-C dataset. For the ImageNet-C dataset, we use the batch size of 64 and the learning rate of 0.00025. All experiments are conducted with one NVIDIA TITAN RTX GPU (24GB). Further implementation details can be found in the supplementary material.

5.1 Quantitative Evaluation and Comparisons

Robustness to corruptions To evaluate the robustness to corruptions, we utilize the pretrained networks on CIFAR10, CIFAR100, TinyImageNet, and ImageNet datasets and validate the pretrained networks on their corresponding corruption datasets, respectively.

Table 1 shows the image classification errors (%) on diverse corruption types with the severest corruption level in CIFAR10-C and CIFAR100-C datasets. Note that TFA and TTT++ are evaluated in the test-time adaptation setting in this experiment. As shown, our proposed method outperforms the baselines on all types of corruptions in both CIFAR10-C and CIFAR100-C datasets with a large margin. We further evaluate our method on a larger dataset, TinyImageNet-C dataset. Table 2 describes the results on the TinyImageNet-C dataset. Similar to the results of CIFAR10-C and CIFAR100-C, CAFA outperforms the baselines in all types of corruptions except for the contrast corruption on the TinyImageNet-C dataset. Finally, we validate our method on a large-scale dataset, ImageNet-C, as reported in Table 3. Unlike different datasets, the classification error of Source is significantly high, making adaptation more challenging than other datasets. For instance, in case of the Gaussian noise corruption, the error is around 96%. Despite such a challenge, ours achieves the lowest averaged error compared to the baselines, improving the Source by around 17%. Furthermore, ours outperforms the previous state-of-the-art TTA method, TENT [47], by 0.6% on average.

Furthermore, in CIFAR10-C and CIFAR100-C datasets, CAFA achieves lower error rates compared to TFA which aligns source and target distributions without considering the class information. Such results demonstrate that considering both intra- and inter-class distances is important when performing feature alignments for test-time adaptation. Note that TFA is originally designed for test-time training (TTT) setting that iterates multiple epochs over test samples.

Office-Home dataset We also evaluate our approach on the Office-Home [61] dataset, which is one of the widely used domain adaptation datasets. We evaluate our method on 12 different adaptation

Table 1: Classification error (%) on the CIFAR10-C (upper group) and CIFAR100-C (lower group) datasets with severity level 5 corruptions. † denotes the results obtained from the official codes, and * indicates the test-time training methods evaluated in the test-time adaptation setting.

Method	Gaus.	Shot	Impu.	Defo.	Glas.	Moti.	Zoom	Snow	Fros.	Fog	Brig.	Cont.	Elas.	Pixe.	Jpeg.	Average
Source	48.73	44.00	57.00	11.84	50.78	23.38	10.84	21.93	28.24	29.41	7.01	13.27	23.38	47.88	19.46	29.14
BN	17.34	16.36	28.25	9.89	26.11	14.27	8.15	16.29	13.82	20.69	8.58	8.49	19.67	11.74	14.17	15.59
PL	17.22	16.07	27.85	9.74	25.94	14.13	8.07	16.12	13.78	20.14	8.53	8.53	19.73	11.65	13.94	15.43
TENT†	15.95	14.55	24.72	9.03	23.25	12.74	7.47	13.91	12.78	16.66	8.13	8.12	18.30	10.85	13.21	13.98
TFA†*	15.80	14.91	23.89	9.29	23.08	12.82	7.41	13.93	12.60	16.41	7.43	7.95	17.24	12.00	12.86	13.84
TTT++†*	16.80	14.92	21.99	9.60	22.97	12.32	7.55	13.14	12.67	14.33	7.06	7.85	17.27	11.63	12.74	13.52
CAFA	14.28	12.70	21.12	7.73	20.84	10.55	6.75	11.93	11.31	13.33	6.95	7.13	16.08	9.59	11.67	12.13
Source	80.77	77.84	87.75	39.62	82.26	54.22	38.38	54.58	60.19	68.11	28.86	50.93	59.54	72.27	49.96	60.35
BN	47.37	45.58	60.10	34.01	56.70	40.99	32.05	46.53	42.57	54.41	32.56	33.30	48.83	37.47	39.43	43.46
PL	46.74	45.26	59.21	33.83	56.08	40.29	31.64	46.10	42.07	53.74	32.24	33.08	48.24	37.11	39.01	43.00
TFA†*	44.68	43.28	56.17	32.47	54.11	37.48	30.32	42.46	39.73	47.57	30.18	32.52	45.34	36.81	37.28	40.69
TTT++†*	43.70	41.84	55.77	31.15	53.38	35.54	29.98	41.13	38.70	45.08	29.14	30.34	44.69	35.47	37.37	39.55
TENT†	43.11	41.70	53.30	31.35	51.08	36.34	29.90	42.73	38.99	45.13	29.64	30.62	44.03	34.23	36.34	39.23
CAFA	41.60	39.77	50.45	30.17	48.35	34.65	28.76	39.52	37.42	41.25	27.95	29.54	42.37	32.87	35.02	37.31

Table 2: Classification error (%) on the TinyImageNet-C dataset with severity level 5 corruptions. † denotes the results obtained from the official codes.

Method	Gaus.	Shot	Impu.	Defo.	Glas.	Moti.	Zoom	Snow	Fros.	Fog	Brig.	Cont.	Elas.	Pixe.	Jpeg.	Average
Source	94.86	93.14	97.25	86.96	88.45	77.87	77.63	83.71	80.35	92.85	81.94	98.55	69.03	58.89	55.64	82.47
BN	68.74	67.80	74.72	68.71	77.13	61.04	59.71	67.37	67.21	76.52	66.09	93.73	61.32	55.07	55.75	68.06
PL	68.11	66.95	74.18	67.92	76.52	60.32	58.87	67.08	66.63	75.99	65.34	93.38	60.82	54.77	55.50	67.49
TENT†	64.11	63.72	70.35	63.22	73.39	56.64	55.07	64.28	62.99	70.39	60.88	92.44	57.17	51.72	52.94	63.95
CAFA	63.68	63.04	70.12	61.27	71.30	55.22	54.34	63.31	61.88	67.96	59.15	92.53	56.16	51.21	52.60	62.92

Table 3: Classification error (%) on the ImageNet-C dataset with severity level 5 corruptions. † denotes the results obtained from the official code.

Method	Gaus.	Shot	Impu.	Defo.	Glas.	Moti.	Zoom	Snow	Fros.	Fog	Brig.	Cont.	Elas.	Pixe.	Jpeg.	Average
Source	95.53	94.93	95.38	84.94	91.66	86.63	77.13	84.06	79.36	77.30	44.30	95.78	85.23	77.40	66.82	82.43
BN	88.31	87.83	87.71	88.42	87.96	78.57	64.42	67.89	69.49	55.22	36.81	89.32	59.21	57.33	67.75	72.42
PL	87.04	87.08	85.91	85.02	86.82	72.27	57.71	59.14	68.46	47.73	34.26	92.51	52.35	48.82	58.40	68.23
TENT†	84.76	82.82	79.55	83.66	86.84	65.84	53.75	55.42	68.46	44.68	34.74	95.03	47.92	44.95	52.90	65.42
CAFA	83.27	80.19	79.23	85.96	86.68	64.53	55.16	54.39	62.93	45.25	35.65	91.91	48.10	45.81	53.14	64.81

scenarios, training a model on one source domain and validating it on other domains. Table 4 shows the image classification errors (%) on different adaptation scenarios of the OfficeHome [61] dataset. As shown, CAFA consistently outperforms the baselines in all scenarios with a large margin. On average, ours reduces the classification error of the Source by around 5%, and that of TENT by around 1.4%.

Table 4: Classification error (%) on the OfficeHome [61] dataset. † denotes the results obtained from the official codes.

Method	Ar→Cl	Ar→Pr	Ar→Re	Cl→Ar	Cl→Pr	Cl→Re	Pr→Ar	Pr→Cl	Pr→Re	Re→Ar	Re→Cl	Re→Pr	Average
Source	67.33	46.68	36.81	68.52	54.22	53.91	66.25	71.25	40.76	45.16	65.02	29.65	53.80
BN	63.34	47.31	36.29	66.09	57.85	54.12	62.22	68.93	39.29	46.27	60.73	30.19	52.72
PL	63.18	46.25	35.87	65.68	56.14	53.16	61.80	68.34	38.51	45.45	60.53	29.62	52.04
TENT†	61.47	44.33	34.82	62.75	52.22	49.16	61.60	66.19	36.26	44.66	58.08	28.14	49.97
CAFA	59.73	42.64	34.01	61.39	51.23	47.69	60.28	63.92	35.87	42.89	54.91	27.84	48.53

Table 5: Digit domain adaptation error (%) from the SVHN dataset to MNIST / MNIST-M / USPS datasets. † denotes that the results are obtained from the official code.

Method	MNIST	MNIST-M	USPS
Source	55.03	56.86	40.66
BN	34.07	62.93	36.52
PL	29.86	61.86	35.48
TENT†	22.31	57.18	33.33
CAFA (Ours)	17.39	53.72	31.72

Digit adaptation For digit adaptation, we train the networks on the SVHN dataset and evaluate the classification errors (%) on MNIST / MNIST-M / USPS datasets. Note that MNIST and USPS consist of grayscale images while MNIST-M is composed of color digit images. Table 5 compares the evaluation results of CAFA and baselines on digit datasets. While previous methods improve the classification errors on MNIST and USPS datasets compared to Source, they show degraded classification accuracy on the MNIST-M dataset. On the other hand, CAFA consistently enhances the adaptation errors on all three datasets with a large margin.

Comparison with baselines from different adaptation settings Even though we address the distribution shifts in the test-time adaptation setting, we compare CAFA with SHOT [37] (source-free

Table 6: Comparison with baselines from different adaptation settings. Classification error (%) is measured in the CIFAR10-C dataset along with the number of step changes. ** indicates the results reported in Liu *et al.* [54].

Test-Time Adaptation				Different Adaptation Tasks	
Method	Step 1	Step 2	Step 3	Method	Error (%)
TENT [†]	13.98	13.72	13.97	SHOT**	14.71
CAFA (Ours)	12.13	11.61	11.79	TFA**	11.87
				TTT++**	9.60

UDA) and TFA and TTT++ [54] (test-time training) as shown in Table 6. Note that we utilize the same pretrained networks used in Liu *et al.* [54], and those methods need to iterate epochs over the test samples several times. For this experiment, we report the averaged classification error over all types of corruptions in the CIFAR10-C dataset. For this experiment, we change the number of loss optimizations for each mini-batch (*i.e.*, the number of steps) in the test-time adaptation setting. We observe both CAFA and TENT achieve the lowest classification errors when the number of steps is two. Additionally, when the number of steps is two, CAFA outperforms SHOT [37] with a large margin, and shows superior performance compared to TFA [54] which utilizes feature alignments without considering class information in the test-time training setting. Although TTT++ [54] shows the best accuracy, it requires a non-trivial amount of computation costs and time since it iterates multiple epochs over test samples.

Table 7: Our ablation results on the CIFAR10-C and CIFAR100-C datasets. The left group shows the effectiveness of considering intra- and inter-class distances, the middle group presents the comparison of updating the batch normalization parameters and full parameters in the feature extractor, and the right group describes the effects of using a tied covariance.

Datasets	Effectiveness of Considering Intra-/Inter-Class Dist.		Updating Batch Norm. vs Full Parameters		Tied Covariance vs Class-wise Covariance	
CIFAR10-C	Source	29.14	Source	29.14	Source	29.14
	TENT [†]	13.98	TENT [†]	13.98	TENT [†]	13.98
	Global FA	19.12	CAFA-Full	12.66	CAFA-Tied	12.47
	Intra-Class Dist. Only	13.02	CAFA	12.13	CAFA	12.13
	CAFA	12.13				
CIFAR100-C	Source	60.35	Source	60.35	Source	60.35
	TENT [†]	39.23	TENT [†]	39.23	TENT [†]	39.23
	Global FA	51.41	CAFA-Full	38.31	CAFA-Tied	38.19
	Intra-Class Dist. Only	41.51	CAFA	37.31	CAFA	37.31
	CAFA	37.31				

5.2 Analysis

Effectiveness of Considering Intra- and Inter-Class Distance

To further validate our motivation for considering intra- and inter-class distances, we compare each component in both CIFAR10-C and CIFAR100-C datasets. As reported in the left group of Table 7, utilizing the global feature alignment performs poorly in TTA. In case of reducing the intra-class distance only, it improves the classification errors on both datasets, but it does not outperform TENT in the CIFAR100-C dataset. Finally, considering both intra- and inter-class distances (CAFA) achieves the lowest classification errors. Such results demonstrate the initial intuition of our work is valid, which is elaborated in Section 1.

Updating the entire parameters of feature extractor In our main experiments, we only update the parameters of batch normalization layers in the feature extractor, following Wang *et al.* [47]. In this ablation study, we further validate CAFA by updating the entire parameters in the feature extractor. Note that since CAFA performs feature alignments using feature vectors, the classifier $h(\cdot)$ cannot be updated by our loss. CAFA-Full in the middle group of Table 7 shows the result of updating the full parameters when utilizing CAFA. While it shows superior performance compared to the baselines, only updating the batch normalization layers outperforms the case of updating the full parameters. As pointed out in Wang *et al.* [47], updating the full model may cause the model to diverge from what they learned from training. Furthermore, we conjecture that the number of samples during test-time adaptation may be not sufficient to optimize the entire parameters to converge.

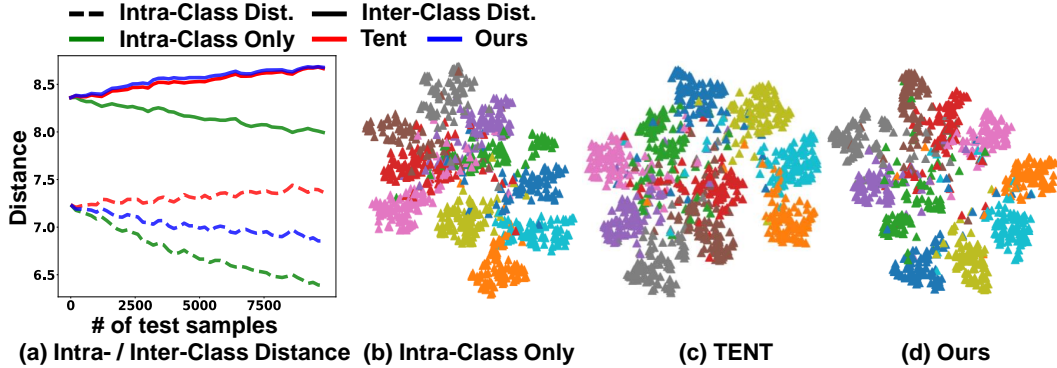


Figure 3: (a) illustrates the change of intra-class distance (dotted lines) and inter-class distance (solid line) as adaptation proceeds. (b-d) show the t-SNE visualizations of applying (b) intra-class distance only, (c) TENT [47], and (d) ours. All visualizations are obtained from the Gaussian noise corruption in the CIFAR10-C dataset.

Impact of using tied covariance We adopt the class-wise covariance matrices for CAFA in the main experiments. However, in linear discriminant analysis (LDA), it is assumed that all the class-conditional Gaussian distributions share the same covariance matrix (*i.e.*, tied covariance). We conduct an ablation study regarding such an issue in the right group of Table 7. We observe that CAFA with tied covariance shows less performance improvement than utilizing the class-wise covariances. We conjecture that it is because class-wise covariances represent the statistics of each class of the source distributions more precisely than the tied covariance. Moreover, as pointed out in Lee *et al.* [60], deep networks are not trained to share the same covariance matrix for all class-conditional distributions. However, regardless of the covariance types, our method still outperforms the existing baselines.

Visualizations To further validate our intuition, we visualize the change of the intra- and inter-class distances in Fig. 3 (a): intra-class distance only (green line), TENT [47] (red line), and CAFA (blue line). As shown in Fig. 3 (a), only reducing the intra-class distance also decreases the inter-class distance, which harms the class-discriminability. In case of TENT [47], we observe that the intra-class distance does not decrease. On the other hand, CAFA desirably reduces the intra-class distance while enlarging the inter-class distance. Such improved class-discriminability is also shown in the t-SNE visualization in Fig. 3 (d). Unlike other methods (Fig. 3 (b) and (c)), ours shows well-separated representation space in a class-wise manner.

6 Discussion

In this work, we proposed a *simple yet effective* feature alignment that considers both intra- and inter-class distances, noting the importance of considering them in test-time adaptation. Most existing feature alignments are generally conducted along with training on the source data, which allows a model to learn target distributions in a class-discriminative manner. However, in case of test-time adaptation where access to the source data is prohibited, a model does not have a chance to learn test features in such a manner. Our simple feature alignment that considers both intra- and inter-class distances effectively addresses such a challenge as shown in our in-depth analysis and extensive experiments. However, there still remains room for improvements: 1) better pseudo-labeling method and 2) better learnable parameters than BN layers. We hope our work inspires the following researchers to investigate more effective test-time adaptation methods.

Pseudo labeling One limitation of our work is that we resort to using the predicted labels when assigning a class to each test sample. This could be problematic in the early phase of adaptation since the model encounters samples of a different distribution, achieving low classification accuracy. Along with our novel perspective to consider both intra- and inter-class distance when performing feature alignment in TTA, we believe that replacing such a pseudo-labeling approach with other advanced methods would further boost the adaptation performance of CAFA.

Finding better learnable parameters than BN layers In our work, we only updated the batch normalization parameters, as also done in Wang *et al.* [47]. Despite its demonstrated effectiveness in TTA, batch normalization parameters only take less than 1% of the model parameters. If we can find better learnable model parameters, it may further improve the adaptation performance of our proposed loss CAFA.

References

- [1] Kaiming He, Xiangyu Zhang, Shaoqing Ren, and Jian Sun. Deep residual learning for image recognition. In *Proceedings of the IEEE conference on computer vision and pattern recognition*, pages 770–778, 2016.
- [2] Ashish Vaswani, Noam Shazeer, Niki Parmar, Jakob Uszkoreit, Llion Jones, Aidan N Gomez, Łukasz Kaiser, and Illia Polosukhin. Attention is all you need. *Advances in neural information processing systems*, 30, 2017.
- [3] Alexey Dosovitskiy, Lucas Beyer, Alexander Kolesnikov, Dirk Weissenborn, Xiaohua Zhai, Thomas Unterthiner, Mostafa Dehghani, Matthias Minderer, Georg Heigold, Sylvain Gelly, et al. An image is worth 16x16 words: Transformers for image recognition at scale. *arXiv preprint arXiv:2010.11929*, 2020.
- [4] Jacob Devlin, Ming-Wei Chang, Kenton Lee, and Kristina Toutanova. Bert: Pre-training of deep bidirectional transformers for language understanding. *arXiv preprint arXiv:1810.04805*, 2018.
- [5] Dan Hendrycks and Thomas Dietterich. Benchmarking neural network robustness to common corruptions and perturbations. *Proceedings of the International Conference on Learning Representations*, 2019.
- [6] Dengxin Dai and Luc Van Gool. Dark model adaptation: Semantic image segmentation from daytime to nighttime. In *2018 21st International Conference on Intelligent Transportation Systems (ITSC)*, pages 3819–3824. IEEE, 2018.
- [7] Georg Volk, Stefan Müller, Alexander Von Bernuth, Dennis Hospach, and Oliver Bringmann. Towards robust cnn-based object detection through augmentation with synthetic rain variations. In *2019 IEEE Intelligent Transportation Systems Conference (ITSC)*, pages 285–292. IEEE, 2019.
- [8] Sungha Choi, Sanghun Jung, Huiwon Yun, Joanne T Kim, Seungryong Kim, and Jaegul Choo. Robustnet: Improving domain generalization in urban-scene segmentation via instance selective whitening. In *Proceedings of the IEEE/CVF Conference on Computer Vision and Pattern Recognition*, pages 11580–11590, 2021.
- [9] Joaquin Quiñero-Candela, Masashi Sugiyama, Anton Schwaighofer, and Neil D Lawrence. *Dataset shift in machine learning*. Mit Press, 2008.
- [10] David Lazer, Ryan Kennedy, Gary King, and Alessandro Vespignani. The parable of google flu: traps in big data analysis. *science*, 343(6176):1203–1205, 2014.
- [11] Konstantinos Bousmalis, George Trigeorgis, Nathan Silberman, Dilip Krishnan, and Dumitru Erhan. Domain separation networks. *Advances in neural information processing systems*, 29, 2016.
- [12] Mingming Gong, Kun Zhang, Tongliang Liu, Dacheng Tao, Clark Glymour, and Bernhard Schölkopf. Domain adaptation with conditional transferable components. In *International conference on machine learning*, pages 2839–2848. PMLR, 2016.
- [13] Mingsheng Long, Han Zhu, Jianmin Wang, and Michael I Jordan. Deep transfer learning with joint adaptation networks. In *International conference on machine learning*, pages 2208–2217. PMLR, 2017.
- [14] Yaroslav Ganin, Evgeniya Ustinova, Hana Ajakan, Pascal Germain, Hugo Larochelle, François Laviolette, Mario Marchand, and Victor Lempitsky. Domain-adversarial training of neural networks. *The journal of machine learning research*, 17(1):2096–2030, 2016.
- [15] Baochen Sun and Kate Saenko. Deep coral: Correlation alignment for deep domain adaptation. In *European conference on computer vision*, pages 443–450. Springer, 2016.
- [16] Yaroslav Ganin and Victor Lempitsky. Unsupervised domain adaptation by backpropagation. In *International conference on machine learning*, pages 1180–1189. PMLR, 2015.
- [17] Haifeng Xia, Handong Zhao, and Zhengming Ding. Adaptive adversarial network for source-free domain adaptation. In *Proceedings of the IEEE/CVF International Conference on Computer Vision*, pages 9010–9019, 2021.
- [18] Jiaxing Huang, Dayan Guan, Aoran Xiao, and Shijian Lu. Model adaptation: Historical contrastive learning for unsupervised domain adaptation without source data. In A. Beygelzimer, Y. Dauphin, P. Liang, and J. Wortman Vaughan, editors, *Advances in Neural Information Processing Systems*, 2021.
- [19] Mingsheng Long, Zhangjie Cao, Jianmin Wang, and Michael I Jordan. Conditional adversarial domain adaptation. *Advances in neural information processing systems*, 31, 2018.

- [20] Rui Shu, Hung Bui, Hirokazu Narui, and Stefano Ermon. A DIRT-t approach to unsupervised domain adaptation. In *International Conference on Learning Representations*, 2018.
- [21] Eric Tzeng, Judy Hoffman, Kate Saenko, and Trevor Darrell. Adversarial discriminative domain adaptation. In *Proceedings of the IEEE conference on computer vision and pattern recognition*, pages 7167–7176, 2017.
- [22] Jungsoo Lee, Jooyeol Yun, Sunghyun Park, Yonggyu Kim, and Jaegul Choo. Improving face recognition with large age gaps by learning to distinguish children. 2021.
- [23] Chaoqi Chen, Weiping Xie, Wenbing Huang, Yu Rong, Xinghao Ding, Yue Huang, Tingyang Xu, and Junzhou Huang. Progressive feature alignment for unsupervised domain adaptation. In *Proceedings of the IEEE/CVF Conference on Computer Vision and Pattern Recognition*, pages 627–636, 2019.
- [24] Shuang Li, Shiji Song, Gao Huang, Zhengming Ding, and Cheng Wu. Domain invariant and class discriminative feature learning for visual domain adaptation. *IEEE transactions on image processing*, 27(9):4260–4273, 2018.
- [25] Kuniaki Saito, Yoshitaka Ushiku, and Tatsuya Harada. Asymmetric tri-training for unsupervised domain adaptation. In *International Conference on Machine Learning*, pages 2988–2997. PMLR, 2017.
- [26] Shaoan Xie, Zibin Zheng, Liang Chen, and Chuan Chen. Learning semantic representations for unsupervised domain adaptation. In *International conference on machine learning*, pages 5423–5432. PMLR, 2018.
- [27] Shai Ben-David, John Blitzer, Koby Crammer, and Fernando Pereira. Analysis of representations for domain adaptation. *Advances in neural information processing systems*, 19, 2006.
- [28] Shai Ben-David, John Blitzer, Koby Crammer, Alex Kulesza, Fernando Pereira, and Jennifer Wortman Vaughan. A theory of learning from different domains. *Machine learning*, 79(1):151–175, 2010.
- [29] Pedro O Pinheiro. Unsupervised domain adaptation with similarity learning. In *Proceedings of the IEEE conference on computer vision and pattern recognition*, pages 8004–8013, 2018.
- [30] Kuniaki Saito, Kohei Watanabe, Yoshitaka Ushiku, and Tatsuya Harada. Maximum classifier discrepancy for unsupervised domain adaptation. In *Proceedings of the IEEE conference on computer vision and pattern recognition*, pages 3723–3732, 2018.
- [31] Judy Hoffman, Eric Tzeng, Taesung Park, Jun-Yan Zhu, Phillip Isola, Kate Saenko, Alexei Efros, and Trevor Darrell. Cycada: Cycle-consistent adversarial domain adaptation. In *International conference on machine learning*, pages 1989–1998. PMLR, 2018.
- [32] Yabin Zhang, Hui Tang, Kui Jia, and Mingkui Tan. Domain-symmetric networks for adversarial domain adaptation. In *Proceedings of the IEEE/CVF Conference on Computer Vision and Pattern Recognition*, pages 5031–5040, 2019.
- [33] Hong Liu, Mingsheng Long, Jianmin Wang, and Michael Jordan. Transferable adversarial training: A general approach to adapting deep classifiers. In *International Conference on Machine Learning*, pages 4013–4022. PMLR, 2019.
- [34] Mingsheng Long, Yue Cao, Jianmin Wang, and Michael Jordan. Learning transferable features with deep adaptation networks. In *International conference on machine learning*, pages 97–105. PMLR, 2015.
- [35] Eric Tzeng, Judy Hoffman, Ning Zhang, Kate Saenko, and Trevor Darrell. Deep domain confusion: Maximizing for domain invariance. *arXiv preprint arXiv:1412.3474*, 2014.
- [36] Eric Tzeng, Judy Hoffman, Trevor Darrell, and Kate Saenko. Simultaneous deep transfer across domains and tasks. In *Proceedings of the IEEE international conference on computer vision*, pages 4068–4076, 2015.
- [37] Jian Liang, Dapeng Hu, and Jiashi Feng. Do we really need to access the source data? source hypothesis transfer for unsupervised domain adaptation. In *International Conference on Machine Learning*, pages 6028–6039. PMLR, 2020.
- [38] Cian Eastwood, Ian Mason, Chris Williams, and Bernhard Schölkopf. Source-free adaptation to measurement shift via bottom-up feature restoration. In *International Conference on Learning Representations*, 2021.

- [39] Rui Li, Qianfen Jiao, Wenming Cao, Hau-San Wong, and Si Wu. Model adaptation: Unsupervised domain adaptation without source data. In *Proceedings of the IEEE/CVF Conference on Computer Vision and Pattern Recognition*, pages 9641–9650, 2020.
- [40] Pietro Morerio, Riccardo Volpi, Ruggero Ragonese, and Vittorio Murino. Generative pseudo-label refinement for unsupervised domain adaptation. In *Proceedings of the IEEE/CVF Winter Conference on Applications of Computer Vision*, pages 3130–3139, 2020.
- [41] Jogendra Nath Kundu, Naveen Venkat, R Venkatesh Babu, et al. Universal source-free domain adaptation. In *Proceedings of the IEEE/CVF Conference on Computer Vision and Pattern Recognition*, pages 4544–4553, 2020.
- [42] Vinod K Kurmi, Venkatesh K Subramanian, and Vinay P Nambodiri. Domain impression: A source data free domain adaptation method. In *Proceedings of the IEEE/CVF Winter Conference on Applications of Computer Vision*, pages 615–625, 2021.
- [43] Hao-Wei Yeh, Baoyao Yang, Pong C Yuen, and Tatsuya Harada. Sofa: Source-data-free feature alignment for unsupervised domain adaptation. In *Proceedings of the IEEE/CVF Winter Conference on Applications of Computer Vision*, pages 474–483, 2021.
- [44] Serban Stan and Mohammad Rostami. Unsupervised model adaptation for continual semantic segmentation. *arXiv preprint arXiv:2009.12518*, 2020.
- [45] Andreas Krause, Pietro Perona, and Ryan Gomes. Discriminative clustering by regularized information maximization. *Advances in neural information processing systems*, 23, 2010.
- [46] Shiqi Yang, Yaxing Wang, Joost van de Weijer, Luis Herranz, and Shangling Jui. Generalized source-free domain adaptation. In *Proceedings of the IEEE/CVF International Conference on Computer Vision*, pages 8978–8987, 2021.
- [47] Dequan Wang, Evan Shelhamer, Shaoteng Liu, Bruno Olshausen, and Trevor Darrell. Tent: Fully test-time adaptation by entropy minimization. In *International Conference on Learning Representations*, 2021.
- [48] Xuefeng Hu, Gokhan Uzunbas, Sirius Chen, Rui Wang, Ashish Shah, Ram Nevatia, and Ser-Nam Lim. Mixnorm: Test-time adaptation through online normalization estimation. *arXiv preprint arXiv:2110.11478*, 2021.
- [49] Fuming You, Jingjing Li, and Zhou Zhao. Test-time batch statistics calibration for covariate shift. *arXiv preprint arXiv:2110.04065*, 2021.
- [50] Marvin Mengxin Zhang, Sergey Levine, and Chelsea Finn. MEMO: Test time robustness via adaptation and augmentation. In *NeurIPS 2021 Workshop on Distribution Shifts: Connecting Methods and Applications*, 2021.
- [51] Steffen Schneider, Evgenia Rusak, Luisa Eck, Oliver Bringmann, Wieland Brendel, and Matthias Bethge. Improving robustness against common corruptions by covariate shift adaptation. *Advances in Neural Information Processing Systems*, 33:11539–11551, 2020.
- [52] Dong-Hyun Lee. Pseudo-label: The simple and efficient semi-supervised learning method for deep neural networks. In *Workshop on challenges in representation learning, ICML*, volume 3, page 896, 2013.
- [53] Yu Sun, Xiaolong Wang, Zhuang Liu, John Miller, Alexei Efros, and Moritz Hardt. Test-time training with self-supervision for generalization under distribution shifts. In Hal Daumé III and Aarti Singh, editors, *Proceedings of the 37th International Conference on Machine Learning*, volume 119 of *Proceedings of Machine Learning Research*, pages 9229–9248. PMLR, 13–18 Jul 2020.
- [54] Yuejiang Liu, Parth Kothari, Bastien van Delft, Baptiste Bellot-Gurlet, Taylor Mordan, and Alexandre Alahi. Ttt++: When does self-supervised test-time training fail or thrive? *Advances in Neural Information Processing Systems*, 34, 2021.
- [55] Sergey Ioffe and Christian Szegedy. Batch normalization: Accelerating deep network training by reducing internal covariate shift. In *International conference on machine learning*, pages 448–456. PMLR, 2015.
- [56] Mingsheng Long, Jianmin Wang, Guiguang Ding, Jiaguang Sun, and Philip S Yu. Transfer feature learning with joint distribution adaptation. In *Proceedings of the IEEE international conference on computer vision*, pages 2200–2207, 2013.
- [57] Philip Haeusser, Thomas Frerix, Alexander Mordvintsev, and Daniel Cremers. Associative domain adaptation. In *Proceedings of the IEEE international conference on computer vision*, pages 2765–2773, 2017.

- [58] Weichen Zhang, Wanli Ouyang, Wen Li, and Dong Xu. Collaborative and adversarial network for unsupervised domain adaptation. In *Proceedings of the IEEE conference on computer vision and pattern recognition*, pages 3801–3809, 2018.
- [59] Ozan Sener, Hyun Oh Song, Ashutosh Saxena, and Silvio Savarese. Learning transferrable representations for unsupervised domain adaptation. *Advances in neural information processing systems*, 29, 2016.
- [60] Dongha Lee, Sehun Yu, and Hwanjo Yu. Multi-class data description for out-of-distribution detection. In *Proceedings of the 26th ACM SIGKDD International Conference on Knowledge Discovery & Data Mining*, pages 1362–1370, 2020.
- [61] Hemanth Venkateswara, Jose Eusebio, Shayok Chakraborty, and Sethuraman Panchanathan. Deep hashing network for unsupervised domain adaptation. In *Proceedings of the IEEE conference on computer vision and pattern recognition*, pages 5018–5027, 2017.
- [62] Yuval Netzer, Tao Wang, Adam Coates, Alessandro Bissacco, Bo Wu, and Andrew Y Ng. Reading digits in natural images with unsupervised feature learning. 2011.
- [63] Yann LeCun, Léon Bottou, Yoshua Bengio, and Patrick Haffner. Gradient-based learning applied to document recognition. *Proceedings of the IEEE*, 86(11):2278–2324, 1998.
- [64] Yaroslav Ganin and Victor Lempitsky. Unsupervised domain adaptation by backpropagation. In *International conference on machine learning*, pages 1180–1189. PMLR, 2015.
- [65] Jonathan J. Hull. A database for handwritten text recognition research. *IEEE Transactions on pattern analysis and machine intelligence*, 16(5):550–554, 1994.
- [66] Alex Krizhevsky, Geoffrey Hinton, et al. Learning multiple layers of features from tiny images. 2009.
- [67] Ya Le and Xuan Yang. Tiny imagenet visual recognition challenge. *CS 231N*, 7(7):3, 2015.
- [68] Jia Deng, Wei Dong, Richard Socher, Li-Jia Li, Kai Li, and Li Fei-Fei. Imagenet: A large-scale hierarchical image database. In *2009 IEEE conference on computer vision and pattern recognition*, pages 248–255. Ieee, 2009.
- [69] Adam Paszke, Sam Gross, Francisco Massa, Adam Lerer, James Bradbury, Gregory Chanan, Trevor Killeen, Zeming Lin, Natalia Gimelshein, Luca Antiga, Alban Desmaison, Andreas Kopf, Edward Yang, Zachary DeVito, Martin Raison, Alykhan Tejani, Sasank Chilamkurthy, Benoit Steiner, Lu Fang, Junjie Bai, and Soumith Chintala. Pytorch: An imperative style, high-performance deep learning library. In H. Wallach, H. Larochelle, A. Beygelzimer, F. d'Alché-Buc, E. Fox, and R. Garnett, editors, *Advances in Neural Information Processing Systems 32*, pages 8024–8035. Curran Associates, Inc., 2019.
- [70] Diederik P. Kingma and Jimmy Ba. Adam: A method for stochastic optimization. In *International Conference on Learning Representations*, 2015.

This supplementary material presents additional experimental results and visualizations of our method, which are not included in the main paper. Section A first describes additional experimental results on CIFAR10-C and CIFAR100-C datasets with different severity levels and the classification accuracy with 5 trials. Section B presents the t-SNE visualizations of our method, CAFA, and TENT [47]. Finally, Section C presents further implementation details.

A Additional Experimental Results

We compare our method, CAFA, to baselines on the CIFAR10-C and CIFAR100-C datasets with different severity levels. As reported in Tables 8-11, CAFA outperforms baselines on all severity levels in the CIFAR10-C and CIFAR100-C datasets. Furthermore, we present the classification errors along with independent trials using different random seeds in Table 12. As shown, CAFA shows minimal performance variation considering the small standard deviation.

B Visualizations

For the qualitative analysis, we visualize the representation space of test samples from our method and TENT [47] by using the t-SNE algorithm. Fig. 4 shows the t-SNE results on different corruption types in the CIFAR10-C dataset, and Fig. 5 illustrates the change of representation space of test samples from our method as adaptation proceeds. As shown, the representations of test samples are well-separated, and they desirably converge in a class-wise manner as adaptation proceeds.

C Further Implementation Details

This section presents further implementation details of our method. We adopt the residual networks [1] with 50 layers (ResNet-50) for all experiments. For the CIFAR10-C [66] dataset, we utilize the same pretrained networks provided by Liu *et al.* [54]. Moreover, we use the pretrained ResNet-50 networks provided by Pytorch [69] for the ImageNet-C [5] experiment. We set the batch size and learning rate as 200 and 0.001, respectively, for all experiments except for the ImageNet-C dataset. For ImageNet-C, we use the batch size of 64 and the learning rate of 0.00025. We adopt Adam [70] optimizer for all experiments, and all experiments are conducted with one NVIDIA TITAN RTX GPU (24 GB). For a fair comparison, all the results are obtained with the same random seed.

Table 8: Classification error (%) on the CIFAR10-C (upper group) and CIFAR100-C (lower group) datasets with severity level 4 corruptions. † denotes the results obtained from the official codes, and * indicates the test-time training methods evaluated in the test-time adaptation setting.

Method	Gaus.	Shot	Impu.	Defo.	Glas.	Moti.	Zoom	Snow	Fros.	Fog	Brig.	Cont.	Elas.	Pixe.	Jpeg.	Average
Source	43.31	34.34	43.78	8.32	52.34	16.72	8.12	19.31	20.07	13.02	5.88	7.45	13.04	26.45	17.12	21.95
BN	15.97	13.14	22.03	8.30	25.85	12.42	7.23	16.99	11.70	13.07	7.49	7.49	13.57	9.25	12.38	13.13
PL	15.81	13.03	21.66	8.21	25.62	12.23	7.18	16.84	11.64	12.88	7.55	7.39	13.59	9.27	12.28	13.01
TENT†	14.51	11.98	19.12	7.69	22.81	10.96	7.10	15.26	11.18	11.03	7.05	7.03	12.69	8.75	11.64	11.92
TFA†*	14.69	12.29	18.03	7.57	22.84	11.19	6.59	14.77	10.48	10.62	6.68	6.89	11.90	9.08	11.03	11.64
TTT++†*	15.20	12.57	17.33	7.61	23.07	10.72	6.62	13.31	10.63	9.87	6.14	6.29	12.13	8.95	11.92	11.49
CAFA	12.73	10.51	16.71	6.66	20.34	9.73	6.07	12.82	9.51	8.98	6.14	6.35	11.25	7.76	10.31	10.39
Source	76.96	69.67	79.91	32.50	82.34	46.32	32.75	50.96	51.77	44.18	26.44	32.44	41.08	52.03	46.34	51.05
BN	44.93	40.95	52.39	31.68	57.40	37.53	30.28	45.78	38.16	41.63	30.30	31.13	40.37	32.93	37.22	39.51
PL	44.54	40.42	51.50	31.63	56.51	37.05	29.95	45.38	37.78	40.93	30.16	30.82	40.04	32.56	36.85	39.07
TFA†*	42.39	37.82	48.26	30.03	54.24	34.70	28.41	41.59	35.60	36.74	28.27	29.78	36.50	31.93	35.62	36.79
TTT++†*	41.16	37.15	47.38	28.74	53.18	32.81	27.95	40.65	34.85	34.30	27.34	27.83	35.41	30.59	34.99	35.62
TENT†	41.28	37.10	46.18	29.06	51.82	33.62	28.08	41.18	35.33	35.01	27.68	28.48	36.12	30.63	34.40	35.73
CAFA	39.11	35.71	44.17	27.83	49.22	32.16	27.56	39.36	34.05	33.22	26.61	27.49	34.97	29.68	33.47	34.31

Table 9: Classification error (%) on the CIFAR10-C (upper group) and CIFAR100-C (lower group) datasets with severity level 3 corruptions. † denotes the results obtained from the official codes, and * indicates the test-time training methods evaluated in the test-time adaptation setting.

Method	Gaus.	Shot	Impu.	Defo.	Glas.	Moti.	Zoom	Snow	Fros.	Fog	Brig.	Cont.	Elas.	Pixe.	Jpeg.	Average
Source	36.96	28.00	26.86	5.73	35.53	16.68	7.54	16.89	18.54	8.98	5.64	6.47	7.69	13.10	15.54	16.68
BN	13.75	11.97	16.01	7.39	16.74	12.36	7.33	14.89	11.63	10.41	7.03	7.23	9.50	8.43	11.51	11.08
PL	13.59	11.90	15.81	7.35	16.58	12.23	7.44	14.75	11.41	10.36	6.97	7.13	9.41	8.32	11.48	10.98
TENT†	12.47	11.29	14.12	6.86	15.47	11.26	6.95	13.40	10.81	9.09	6.52	6.87	8.99	7.93	10.84	10.19
TFA†*	12.71	11.00	13.56	6.65	14.96	10.96	6.72	12.76	10.30	8.77	6.35	6.49	8.33	7.81	10.42	9.85
TTT++†*	13.41	11.16	12.71	6.18	15.14	10.55	6.45	11.87	10.32	7.78	5.80	6.11	8.38	7.36	10.80	9.60
CAFA	10.90	10.01	11.89	5.95	13.23	9.77	5.99	11.38	9.47	7.54	5.93	6.28	8.00	7.19	9.60	8.88
Source	71.80	63.00	65.65	26.15	73.00	46.43	31.03	48.51	48.84	35.35	25.45	28.77	30.76	38.34	43.74	45.12
BN	41.70	38.35	43.93	29.59	44.93	37.70	29.89	42.60	37.45	37.00	29.72	30.52	34.24	31.80	35.40	36.32
PL	41.26	38.08	43.45	29.59	44.68	37.35	29.69	42.33	37.33	36.50	29.55	30.21	33.80	31.58	35.11	36.03
TFA†*	39.27	35.77	40.52	27.98	42.05	34.99	28.51	38.72	35.01	32.90	27.83	28.81	31.43	30.60	34.38	33.92
TTT++†*	38.39	34.51	38.95	26.52	41.53	33.65	27.64	37.75	34.06	31.32	26.78	27.22	30.18	29.46	33.26	32.75
TENT†	38.37	34.72	39.50	27.41	40.91	33.81	27.99	39.10	34.69	31.97	27.36	27.94	31.80	29.09	32.94	33.17
CAFA	36.97	33.53	37.41	26.21	38.96	32.46	27.26	36.82	33.64	30.13	26.53	27.07	30.20	28.23	32.05	31.83

Table 10: Classification error (%) on the CIFAR10-C (upper group) and CIFAR100-C (lower group) datasets with severity level 2 corruptions. † denotes the results obtained from the official codes, and * indicates the test-time training methods evaluated in the test-time adaptation setting.

Method	Gaus.	Shot	Impu.	Defo.	Glas.	Moti.	Zoom	Snow	Fros.	Fog	Brig.	Cont.	Elas.	Pixe.	Jpeg.	Average
Source	24.43	14.91	18.87	5.32	37.16	11.58	6.75	18.33	11.29	6.76	5.38	5.94	7.06	10.35	14.42	13.24
BN	11.24	8.92	12.66	7.13	16.28	10.17	7.08	12.77	9.45	8.43	7.02	7.14	9.50	8.35	10.71	9.79
PL	11.17	8.81	12.71	6.92	16.27	10.10	7.15	12.67	9.43	8.41	7.02	6.96	9.45	8.31	10.66	9.74
TENT†	10.52	8.15	11.45	6.65	15.03	9.64	6.67	11.18	8.69	7.44	6.50	6.72	8.80	7.82	9.85	9.01
TFA†*	10.29	8.09	10.85	6.35	14.87	8.97	6.43	11.29	8.27	7.47	6.21	6.40	8.39	7.42	9.61	8.73
TTT++†*	10.47	7.96	10.16	5.89	14.92	8.63	6.26	10.40	8.26	6.80	5.78	5.86	7.84	7.07	9.75	8.40
CAFA	9.22	7.51	9.65	5.78	13.22	8.20	5.86	9.71	7.57	6.55	5.87	6.02	7.64	6.95	8.90	7.91
Source	59.17	44.40	54.99	24.91	73.55	37.45	28.70	49.25	37.83	29.75	25.01	26.84	29.35	34.25	41.17	39.77
BN	37.60	33.23	39.55	29.11	44.32	33.91	29.63	38.89	33.89	33.74	29.05	29.74	33.21	30.94	34.03	34.06
PL	37.40	32.92	39.01	28.88	43.91	33.56	29.45	38.67	33.68	33.42	28.86	29.48	32.90	30.71	33.82	33.78
TFA†*	35.27	31.10	36.71	27.86	42.04	32.00	28.65	36.03	31.18	30.22	27.60	28.32	30.65	29.30	33.11	32.00
TTT++†*	33.60	29.74	34.88	25.90	41.21	30.64	26.97	34.86	30.17	28.89	26.19	26.68	29.57	28.29	31.84	30.63
TENT†	34.29	30.72	35.37	27.22	40.35	31.03	27.54	35.55	31.05	29.80	26.84	27.60	30.54	28.43	31.82	31.21
CAFA	33.02	29.38	33.75	26.09	38.34	29.63	26.73	33.47	29.79	28.18	25.94	26.45	29.58	27.64	30.95	29.93

Table 11: Classification error (%) on the CIFAR10-C (upper group) and CIFAR100-C (lower group) datasets with severity level 1 corruptions. † denotes the results obtained from the official codes, and * indicates the test-time training methods evaluated in the test-time adaptation setting.

Method	Gaus.	Shot	Impu.	Defo.	Glas.	Moti.	Zoom	Snow	Fros.	Fog	Brig.	Cont.	Elas.	Pixe.	Jpeg.	Average
Source	14.00	10.09	11.62	5.24	38.69	7.75	7.40	9.48	8.14	5.74	5.37	5.47	7.69	6.69	10.51	10.26
BN	8.89	8.08	10.17	7.04	16.16	8.55	7.55	9.44	7.66	7.47	7.00	6.92	9.81	7.50	8.76	8.73
PL	8.83	7.90	10.17	6.94	16.05	8.42	7.59	9.40	7.54	7.41	6.93	6.81	9.77	7.38	8.70	8.66
TENT†	8.25	7.50	9.71	6.54	14.75	7.94	7.15	8.71	6.94	6.62	6.43	6.48	9.35	7.29	8.37	8.14
TFA†*	7.94	7.24	8.95	6.26	14.38	7.63	7.11	8.37	7.10	6.45	6.23	6.02	8.64	6.75	7.69	7.79
TTT++†*	8.23	6.97	8.52	5.61	15.17	7.43	6.84	7.66	6.55	5.95	5.61	5.80	8.39	6.65	7.86	7.55
CAFA	7.37	6.54	8.36	5.80	13.07	6.99	6.34	7.84	6.38	6.04	5.70	5.76	8.03	6.35	7.44	7.20
Source	42.81	35.37	40.39	24.70	74.15	31.29	29.80	35.16	31.07	25.20	24.79	25.23	30.04	28.64	34.83	34.23
BN	32.74	30.64	34.21	28.69	44.57	32.11	30.34	33.10	30.59	29.69	28.55	28.90	34.23	29.94	31.52	31.99
PL	32.61	30.50	33.70	28.52	44.10	31.83	30.19	32.82	30.52	29.25	28.46	28.61	33.84	29.72	31.27	31.73
TFA†*	30.64	28.78	31.88	27.43	41.80	30.58	29.04	30.70	29.27	27.84	27.31	27.56	31.11	28.58	30.29	30.19
TTT++†*	29.63	28.25	30.33	25.63	41.00	29.07	27.36	29.76	27.81	26.35	26.17	26.14	30.11	27.34	29.15	28.94
TENT†	30.07	28.53	31.01	26.84	40.33	29.45	28.18	30.56	28.49	27.14	26.71	27.07	31.33	27.76	29.12	29.51
CAFA	28.82	27.70	30.09	25.84	38.38	28.02	27.09	29.06	27.36	26.23	25.80	25.91	30.33	26.94	28.63	28.41

Table 12: Classification error (%) on the severity level 5 corruptions in the CIFAR10-C dataset with different random seeds.

Trial	Gaus.	Shot	Impu.	Defo.	Glas.	Moti.	Zoom	Snow	Fros.	Fog	Brig.	Cont.	Elas.	Pixe.	Jpeg.	Average
0	14.05	13.06	21.35	8.07	20.45	11.10	6.96	11.92	11.31	13.22	7.06	7.14	16.05	9.65	11.70	12.21
1	13.79	12.90	21.05	8.13	21.08	10.85	6.92	11.92	11.20	13.10	6.83	7.22	16.03	9.63	11.57	12.15
2	14.07	12.60	21.01	7.89	20.73	10.71	6.86	11.87	11.24	13.46	6.92	6.94	16.16	9.80	11.55	12.12
3	13.80	12.99	20.83	8.00	20.62	10.55	6.71	11.89	11.64	13.68	7.11	7.04	16.22	9.82	11.25	12.14
4	13.70	12.71	21.07	8.09	20.94	10.68	6.87	11.96	11.41	13.82	7.04	7.05	15.90	9.67	11.68	12.17
std	0.17	0.19	0.19	0.09	0.25	0.21	0.10	0.03	0.18	0.30	0.11	0.11	0.12	0.09	0.18	0.03

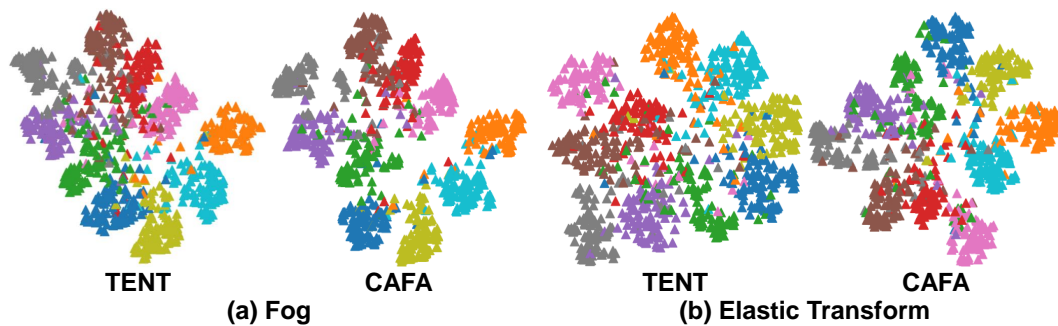


Figure 4: t-SNE visualizations of ours (CAFA) and TENT from (a) Fog and (b) Elastic Transform corruptions with severity level 5 in the CIFAR10-C dataset.

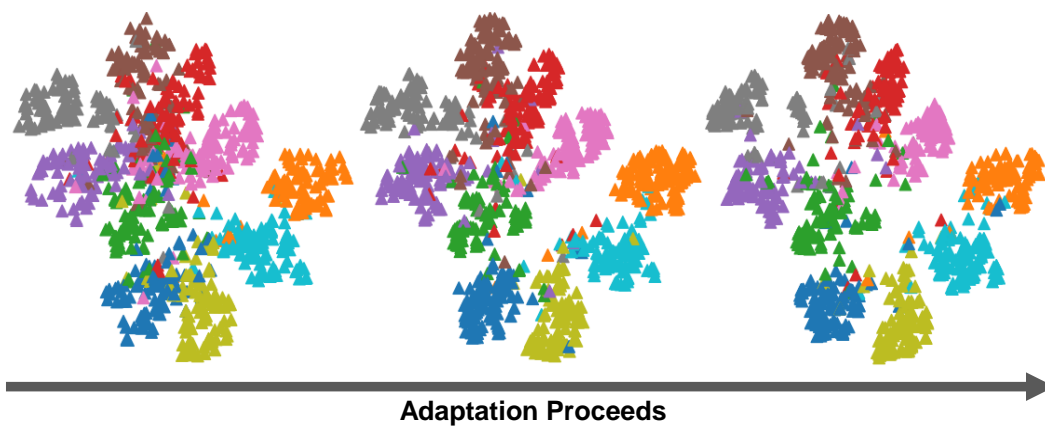


Figure 5: Change of the representation space of test samples from our method as adaptation proceeds. Representation space is visualized by the t-SNE algorithm, and visualizations are obtained from the Fog corruption with severity level 5 in the CIFAR10-C dataset.